

Crystallization kinetics of calcium oxalate hydrates studied by scanning confocal interference microscopy

Bernd Grohe^a, Kem A. Rogers^d, Harvey A. Goldberg^{a,b,c}, Graeme K. Hunter^{a,b,c,*}

^aCIHR Group in Skeletal Development & Remodelling, Schulich School of Medicine & Dentistry, University of Western Ontario, London, Ont., Canada N6A 5C1

^bDivision of Oral Biology, Schulich School of Medicine & Dentistry, University of Western Ontario, London, Ont., Canada N6A 5C1

^cDepartment of Biochemistry, Schulich School of Medicine & Dentistry, University of Western Ontario, London, Ont., Canada N6A 5C1

^dDepartment of Anatomy & Cell Biology, Schulich School of Medicine & Dentistry, University of Western Ontario, London, Ont., Canada N6A 5C1

Received 20 January 2006; received in revised form 20 July 2006; accepted 30 July 2006

Communicated by T.F. Kuech

Abstract

Scanning confocal interference microscopy (SCIM) is an optical technique that allows the visualization of structures below the limits of classical optical microscopy ($\ll 250$ nm). This study represents the first use of SCIM to analyze the formation of calcium oxalate crystals, the major constituent of kidney stones. Crystals were nucleated and grown on the glass bottom of Petri dishes in the presence and absence of the polyelectrolyte inhibitor poly-L-aspartic acid (poly-asp). In the absence of poly-asp, monoclinic calcium oxalate monohydrate (COM) nucleated from $\{100\}$ or $\{010\}$ faces. The first observed particles were 70–120 nm in diameter and grew by a step-like progression in the $[001]$ and $[010]$ directions. Addition of poly-asp had several effects on calcium oxalate formation. First, the number of particles was increased, but their sizes were decreased. Second, the rate of COM growth in the $[001]$ direction was decreased to a greater extent than the rate along $[010]$. Third, the formation of tetragonal calcium oxalate dihydrate (COD) crystals was favored. Fourth, the rates of COD growth along $\langle 110 \rangle$ and allied directions were decreased, whereas that parallel to $\langle 001 \rangle$ is increased.

Sequences of highly resolved growth fronts show step displacement for COM and moving crystal edges for COD. Analysis of image sequences suggested that growth is strongly affected by competing and alternating processes, in which diffusion processes are rate-limiting and induce nonlinear growth. This study shows that SCIM is a powerful technique for the quantitative analysis of crystallization processes and for determining the mode of action of inhibitors.

© 2006 Elsevier B.V. All rights reserved.

PACS: 61.66.Fn; 81.10.Dn; 87.64.Td; 87.68.+z

Keywords: A1. Biomineralization; A1. Calcium oxalate monohydrate (COM); A1. Confocal interference microscopy; A1. Crystal growth; A1. Polyelectrolyte inhibitor; A2. Calcium oxalate dihydrate (COD)

1. Introduction

Over the last century the occurrence of kidney and ureteric stones has increased [1] with a decreasing age of onset [2] and high recurrence rates [1]. Urolithiasis there-

fore has become a significant health issue. Most kidney stones are found in the upper urinary tract, and the majority ($\sim 80\%$) contains calcium oxalate (CaOx) as their primary mineral phase [3–6].

The formation of kidney stones is thought to be a complex process involving a number of factors. Nucleation and growth of calcium oxalate crystals in urine is affected by the level of supersaturation of Ca^{2+} and $\text{C}_2\text{O}_4^{2-}$; by a variety of urinary components, such as proteins and citrate; and by interactions with the kidney epithelium. Urinary proteins can act as inhibitors of nucleation and crystal

*Corresponding author. CIHR Group in Skeletal Development and Remodeling, Schulich School of Medicine & Dentistry, University of Western Ontario, London, Ont., Canada N6A 5C1. Tel: +1 519 661 2185; fax: +1 519 850 2459.

E-mail addresses: bgrohe@uwo.ca (B. Grohe), graeme.hunter@schulich.uwo.ca (G.K. Hunter).

growth as well as crystal aggregation. The ability of calcium oxalate crystals to give rise to a stone therefore depends upon the prevailing conditions for crystal growth, crystal aggregation and interactions with the epithelial cells lining the nephrons [7–10].

While both calcium oxalate monohydrate (COM) and dihydrate (COD) can be formed in urine or at epithelial cell surfaces, several studies have shown that COM has a greater tendency to form stones than COD [4–6,11]. In addition, it was found that COM crystals either nucleate at or bind rapidly to the surface of kidney epithelia cells in culture. These crystals are then internalized, suggesting a mechanism whereby crystals could be retained in the renal tissue of stone-forming patients [9,12,13].

Certain urinary proteins have been shown to inhibit CaO_x crystal formation [14,15], block the adhesion of crystals to cells and other crystals [16] or favor the formation of COD [11,17]. Osteopontin (OPN) was found to be the most potent inhibitor of CaO_x crystal formation in human urine [18,19]. OPN is rich in aspartic and glutamic acids and has numerous sites of serine and threonine phosphorylation [19–21]. A contiguous sequence of 8–10 aspartic acid residues is believed to be important for mediating interactions with crystal surfaces [22,23].

The effects of OPN and other inhibitors on calcium oxalate crystallization have been investigated by a number of different methods. Many studies have used light or scanning electron microscopy (SEM) to analyze shapes and sizes of crystals at various stages of a reaction [24,25]. However, the resolution of light microscopy is too low to visualize crystallization of small crystals and SEM cannot be used to study growing crystals in vitro. Crystal formation can also be quantified by indirect methods such as following the decay of supersaturation [26] or the increase in turbidity [3]. These methods, however, do not provide information about growth of individual crystals [3,27,28]. Recently, atomic force microscopy (AFM) has been used to study COM growth processes [29–31]. Using this technique, Qiu et al. [29] reported that OPN inhibits the growth of steps on $\{010\}$ faces of COM crystals to a greater extent than on $\{001\}$ or $\{100\}$ faces. In contrast, poly-L-aspartic acid (poly-asp) inhibits growth parallel to $\langle 001 \rangle$, reflecting preferred adsorption to $\{001\}$ and/or $\{121\}$, whereas poly-glutamic acid shows a higher affinity to $\{010\}$ faces [30,31]. However, AFM requires a direct interaction between a cantilever tip and a surface, which may affect growth and/or adsorption processes [32,33].

In contrast, scanning confocal interference microscopy (SCIM) allows noninvasive imaging and real-time analysis at moderately high resolution. The high resolution results from (a) the optimized pinhole diameter of the confocal microscope and (b) the imaging of enhanced contrast variations induced by interfering light beams reflected from surfaces such as crystal faces and growth steps. As a result, a lateral resolution of $\lambda/3$ and an axial resolution of $\lambda/8$ can be achieved (where λ is the wavelength of the laser light used). In other words, objects with a lateral separation of

30–100 nm can be imaged, depending on the wavelength of the laser used [34,35].

In the present study, we use SCIM to measure growth rates of COM and COD crystals along different axes and to study the effects of the model inhibitor poly-asp on crystal formation. A detailed analysis of the data obtained reveals effects of poly-asp on growth at different crystal faces and on the development of growth steps. These findings illustrate the potential of SCIM for the quantitative analysis of crystal growth processes.

2. Materials and experimental methods

2.1. Chemicals and solution preparation

Reagent grade sodium oxalate ($\text{Na}_2\text{C}_2\text{O}_4$; J.T. Baker), calcium nitrate tetra-hydrate ($\text{Ca}(\text{NO}_3)_2 \cdot 4\text{H}_2\text{O}$; J.T. Baker), sodium chloride (NaCl ; J.T. Baker), sodium acetate (CH_3COONa , anhydrous; Sigma) and poly-asp (sodium salt, ~ 9.15 kDa; Sigma) were used as obtained. Deionized water purified with a Milli-Q water system (Millipore filters) and filtration through a $0.2 \mu\text{m}$ pore size membrane was used for the preparation of all solutions. Calcium and oxalate stock solutions, either 5 mM (stock i for end concentrations of 1 mM) or 10 mM (stock ii for end concentrations of 2 mM), were prepared by adding 25 mM sodium acetate and 375 mM sodium chloride, respectively. For calcium stocks i and ii the final pH was 7.3, whereas both oxalate stocks (i and ii) showed a pH of 6.1. In addition, aqueous stock solutions of poly-asp of 1 mg/ml and 50 $\mu\text{g}/\text{ml}$ were mixed.

2.2. In-situ crystallization

Glass-bottomed Petri dishes (polystyrene dish: diameter: 35 mm; glass bottom: grade no.: 1.5; diameter: 10 mm; MatTek) and all reaction solutions were preheated to $37 \pm 0.2^\circ\text{C}$. The Petri dishes were placed in a heated insert assembled on the stage of a Zeiss LSM 410 confocal microscope and oxalate solutions added to the dishes followed by water and calcium solutions.

To obtain equimolar concentrations of calcium and oxalate of 1 mM, (low ion concentrations, LIC), oxalate stock i, calcium stock i and water were mixed at ratios of 1:1:3. For final calcium and oxalate concentration of 2 mM each (high ion concentrations, HIC), oxalate stock ii, calcium stock ii and water were added at the same ratios (1:1:3). The total volume of reaction solutions was always 4 ml. If poly-asp solutions were used, the volume of water was correspondingly reduced. Crystallization was allowed to proceed for 30–50 min (unless otherwise noted). For representative reactions, pH measurements were carried out immediately after mixing the solutions. Variations of calcium oxalate concentrations (LIC or HIC) and the absence or presence of poly-asp (up to 500 $\mu\text{g}/\text{ml}$) did not influence the pH values significantly: the pH was always between 6.65–6.75.

2.3. SCIM method

The method is based on (a) the optimized pinhole diameter of a confocal microscope leading to a strict two-dimensional map of the objects within the scanning plane and (b) the use of enhanced contrast variations induced by interfering light beams reflected from surfaces such as crystal faces and growth steps. Interference occurs if the substrate and the crystal phase are optically transparent and if they have a higher refractive index than the thin film (solution) in between both phases [36–39]. The phenomenon is based on multiple reflections at layered structures in thin films and can be described by Fresnel equations specified in classical optics [37].

2.4. SCIM imaging

All precipitates were scanned and imaged using a helium/neon-laser (wavelength: $\lambda = 632.8$ nm), a 63x planapo achromat oil immersion objective, a 90/10 mirror and the LSM 410 software (Carl Zeiss). Prior to every experiment, a pre-alignment of the microscope was carried out and the focus adjusted to the interface between glass and reaction solution. After adding the last solution (Ca^{2+}), nucleating and growing crystals were imaged every 5 s for 30 min, unless otherwise noted. If necessary, a fine-tuning of the focus was conducted during imaging to maintain the focal plane at the crystal–glass interface. All images represent surfaces of crystals generated at the crystal–glass interface.

In order to identify the generated crystal phases, shapes, and morphologies image sequences were evaluated by molecular and crystal data [25,30,31,40–42] and by a calculation routine [43]. For examination of generation rates and growth kinetics three image sequences of replicate samples were taken and growth developments measured by a ruler. Growth rate–time diagrams were derived from crystal size–time curves.

3. Results

3.1. Effect of reaction conditions on generated crystal morphologies and phases

Experiments performed in glass-bottomed Petri dishes and in the presence or absence of poly-asp were carried out to image and investigate in-situ precipitating phases and morphologies. In addition to control reactions (without additives), syntheses were carried out at LIC in the presence of 2 and 6 $\mu\text{g}/\text{ml}$ poly-asp and at HIC using 20, 60, 100 and 200 $\mu\text{g}/\text{ml}$ poly-asp.

At LIC and HIC, controls showed the formation of well-faceted COM crystals (Fig. 1a). However, the generation of COD was rarely detected under these conditions with only three bipyramidal COD crystals observed in 2 of the 14 replicate samples at LIC (Fig. 1b). At HIC, COD was not found, at all. Other crystal phases, such as calcium

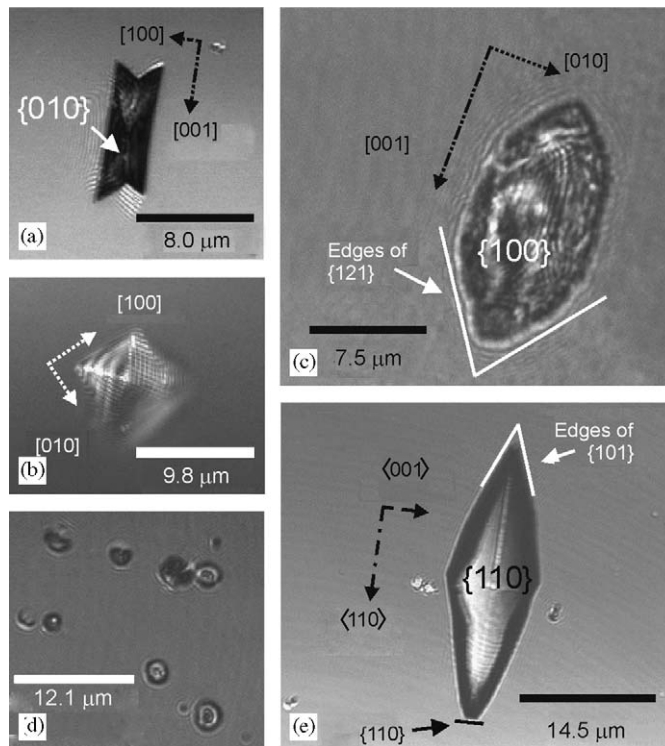


Fig. 1. SCIM images of COM and COD morphologies generated in the absence or presence of poly-asp at LIC and HIC. (a) HIC, no poly-asp: well-faceted COM; (b) LIC, no poly-asp: bipyramidal COD (imaged parallel to $[001]$), without forming a crystal–glass interface; (c) LIC, 2 $\mu\text{g}/\text{ml}$ poly-asp: COM showing rounded shapes and 72° -angles at both ends of the crystal (white lines) between edges of $\{121\}$ planes bounding $\{100\}$ planes [25,31]. (d) LIC, 6 $\mu\text{g}/\text{ml}$ poly-asp: donut-shaped COM; (e) HIC, 20 $\mu\text{g}/\text{ml}$ poly-asp: COD generating a $\{110\}$ crystal–glass interface. The white lines indicate 40° -angles between edges of $\{101\}$ or $\{011\}$ planes bounding $\{110\}$ edges at both ends of the crystal [42,43].

oxalate trihydrate, were never detected, either at LIC or at HIC.

The addition of poly-asp induced similar changes to the morphology of COM at both LIC and HIC. However, higher concentrations of poly-asp were required at HIC. Well-faceted COM changed to morphologies characterized by rounded edges (Fig. 1c) and, at higher poly-asp concentrations, to donut shapes (Fig. 1d). The round-edged COM shown in Fig. 1c still exhibits 72° angle between the $\{121\}$ planes (not visible) binding the $\{100\}$ faces at both ends of the crystal, which is a feature of well-faceted COM. COD crystals developed (100) and (010) faces in the presence of 2 $\mu\text{g}/\text{ml}$ poly-asp or higher at LIC, or in the presence of 20 $\mu\text{g}/\text{ml}$ poly-asp or higher at HIC. This led to the formation of $\{110\}$ edges (Fig. 1e). COD elongation along the c -axis, which results in the formation of tetragonal $\{100\}$ prisms with pyramidal end caps, could be observed at concentrations of 100 $\mu\text{g}/\text{ml}$ poly-asp and above (not shown).

3.2. Crystallization kinetics

The incubation time required to observe the first crystals, varied from 2–17 min. This time span was dependent upon

calcium oxalate concentrations (HIC or LIC) rather than on poly-asp concentrations, and showed shorter incubation times at HIC. In contrast, poly-asp significantly influenced nucleation rates. Increasing poly-asp concentrations resulted in increased particle number densities and smaller particle sizes (see Fig. 1d). The precipitation of crystals occurred during the entire reaction time, independent of poly-asp additions.

3.2.1. Nucleation and growth of COM

For analysis of precipitating crystals, measurements began when a microscopic field containing a COM crystal was encountered. Due to the high resolution of the imaging method, crystals as small as $0.07\text{--}0.12\ \mu\text{m}$ could be detected. Here, the aligned focus of the microscope and the ability to suppress background noise during mapping were the major factors that determined the effective resolution.

Fig. 2 shows an image sequence of a nucleating and growing COM crystal under control conditions at HIC. The crystal nucleated 2 min after starting the reaction. By 25–30 s after nucleation, the crystal had already grown $2.7 \pm 0.1\ \mu\text{m}$ along $[001]$ (Fig. 2c); by 5 min, it measured $14.2 \pm 0.1\ \mu\text{m}$ in the $[001]$ direction (Fig. 2g). Crystals nucleated at later times grew more slowly ($0.5\text{--}1.5\ \mu\text{m}/\text{min}$) during the first 5 min, presumably due to the lower supersaturation (Figs. 3a, b). In contrast, initial growth (first 5 min) parallel to $[010]$ showed rates between 0.55 and $1.2\ \mu\text{m}/\text{min}$ for early nucleated crystals (Fig. 2) and rates between 0.1 and $1.0\ \mu\text{m}/\text{min}$ for later-nucleated crystals (Figs. 3a, b). At LIC, growth rates were lower than those at HIC. COM crystallized under control conditions showed growth rates between 0.25 and $0.75\ \mu\text{m}/\text{min}$ along $[001]$ and rates between 0.1 and $0.5\ \mu\text{m}/\text{min}$ parallel to $[010]$ during the initial period of growth (first 5 min; Figs. 3d,e). It should be noted that crystals nucleated after both short (< 5 min) and long lag times (> 15 min) had similar final sizes (after ~ 25 min). It seems that rapid growth at high supersaturation is followed by moderate growth after supersaturation decreases to a

certain level. At both calcium oxalate concentrations (HIC and LIC) the width-to-length ratio of crystals changed with increasing reaction time, showing a decrease of the aspect ratios in $[010]/[001]$ directions from 1 (at nucleation) to ~ 0.34 at the end of the elapsed time. Thus, growth along $[001]$ was faster than growth along $[010]$, and final aspect ratios ($0.32\text{--}0.36$) were not controlled by incubation times or, more precisely, by supersaturations (Figs. 3a, b, d, e). The growth curves also feature sequences of increased and decreased growth along $[010]$ and $[001]$ with time, resulting in step-like curve progressions. These discontinuities were more frequent during growth at higher supersaturations such as initial growth after nucleation and crystal growth after short lag times (Figs. 4a, c).

In contrast to COM of controls, the presence of poly-asp drastically decreased growth rates along $[001]$, whereas the rates in $[010]$ directions remained initially similar to those of controls, but increased at later stages of reactions (Figs. 3c, f and 4b, d). This behavior could be observed up to $6\ \mu\text{g}/\text{ml}$ poly-asp, the highest concentration used at LIC, and at $20\ \mu\text{g}/\text{ml}$ poly-asp at HIC. However, higher poly-asp concentrations ($60, 100$ and $200\ \mu\text{g}/\text{ml}$) used at HIC led to decreased growth rates in $[001]$ directions as well as in $[010]$ directions (not shown). The presence of inhibitor also affected aspect ratios. With $6\ \mu\text{g}/\text{ml}$ poly-asp at LIC or $20\ \mu\text{g}/\text{ml}$ poly-asp at HIC, the final aspect ratio decreased only slightly from 1 (at nucleation) to $\sim 0.8\text{--}0.9$ (Figs. 3c, f). Poly-asp concentrations $> 20\ \mu\text{g}/\text{ml}$ at HIC resulted in growth of donut shapes (see also Section. 3.1), and consequently in constant aspect ratios of 1 (not shown). The step-like growth curves found for crystals grown under control conditions could also be observed in the presence of inhibitor, however, this growth behavior was rather suppressed (Figs. 3c, f and 4b, d).

More insight into the growth of COM is provided by Fig. 5, which shows an image sequence of the growth front of a COM crystal grown at LIC in the presence of $2\ \mu\text{g}/\text{ml}$ poly-asp. In contrast to well-faceted COM of controls (see Section 3.1), rounded crystal edges were generated, which became even more rounded during the reaction. Here, initial

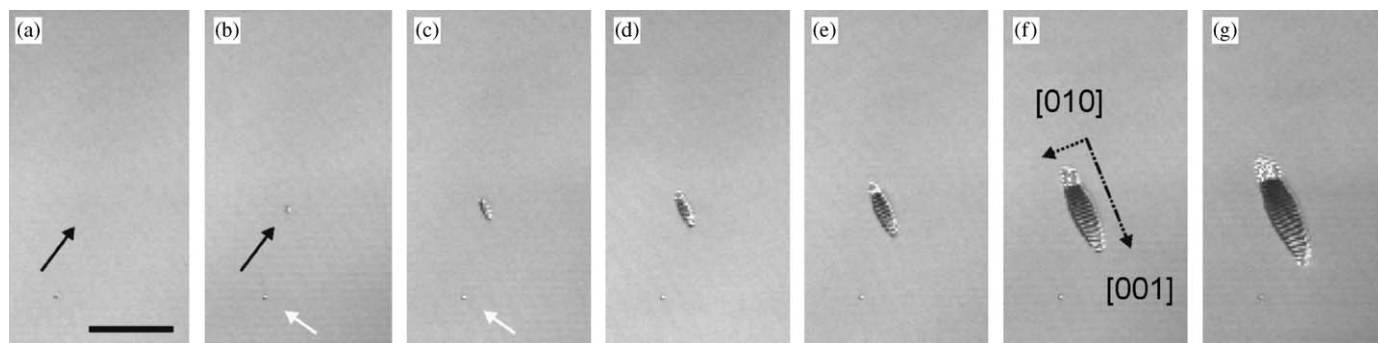


Fig. 2. SCIM image sequence of a precipitating COM at HIC (no poly-asp). Scale bar: $10\ \mu\text{m}$. Incubation time: 2 min. (a)–(c) Nucleation and first stages of growth (30 s). Time between (a) and (b): 5 s. Black arrow: nucleation site. White arrow: artifact present throughout the imaged reaction. (d)–(g) Crystal growth imaged after: (d) 55 s, (e) 1 min 45 s, (f) 3 min 25 s and (g) 5 min 5 s. The sequences of black and white stripes represent interference patterns resulting from destructive and constructive interference.

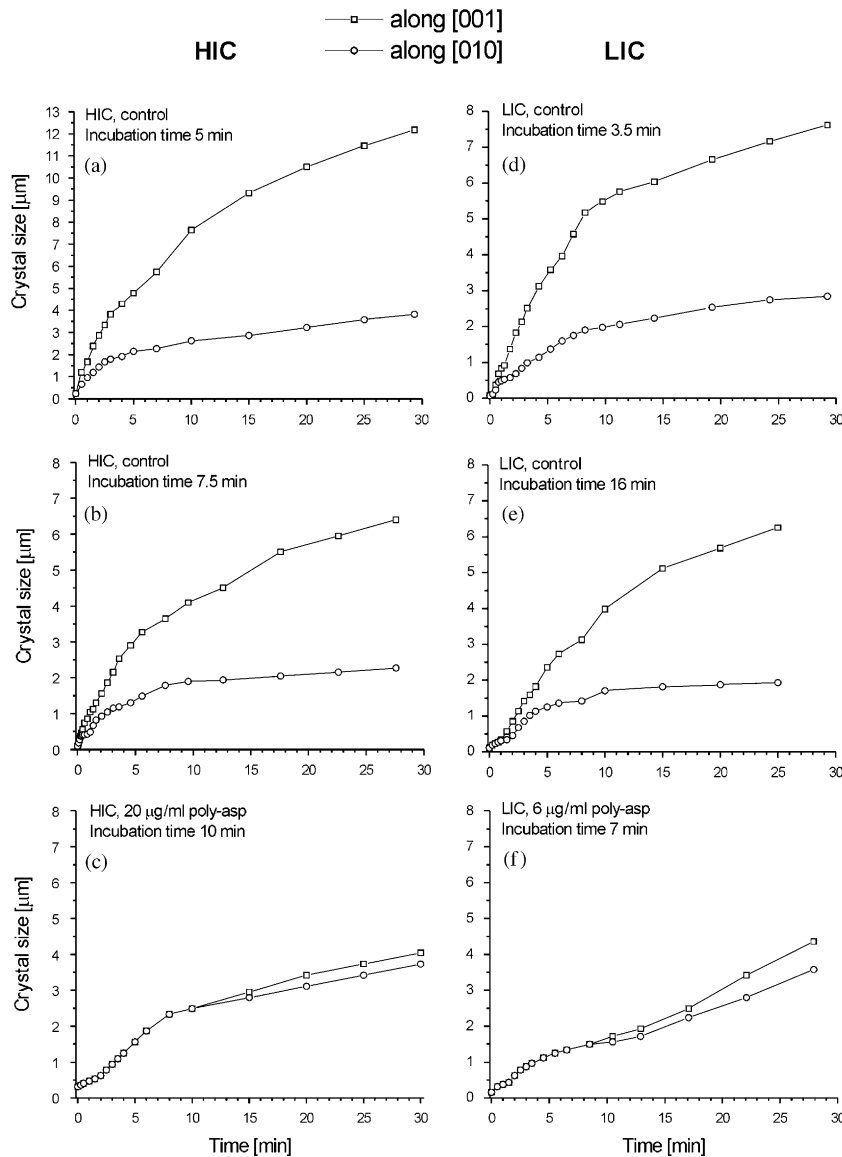


Fig. 3. Effect of supersaturation and poly-asp on COM growth along [001] and [010]. Error of measurement $\pm 0.05 \mu\text{m}$. (a),(b) and (d),(e) Crystals nucleated after long lag times (corresponding to lower supersaturations) exhibit decreased crystal growth along [001] and [010], while final aspect ratios are nearly independent from supersaturations, showing values of ~ 0.34 for [010]/[001] ratios. (c), (f) The presence of poly-asp results in a decreased growth along [001] and increased growth rates parallel to [010], leading to aspect ratios of 0.8–0.9 at the end of the reaction time. (a)–(f) Growth curves exhibit step-like face displacements in both growth directions being more pronounced at high supersaturations and low (or no) poly-asp additions.

growth (first 12 min) was accompanied by the formation and displacement of steps, but also by the decay of such growth steps (integration of steps into the crystal matrix). Later reaction times showed less step conversion but an enhanced step development and displacement (last ~ 18 min; see area in front of the black arrow in Fig. 5). This part of the growth process also revealed slightly higher displacement velocities along [010] compared to [001] direction.

3.2.2. Nucleation and growth of COD

Under control conditions at LIC, growth of COD from an initial nucleus appears to occur virtually instantaneously. The crystal shown in Fig. 1b, for example, grew to the size shown during ~ 1 min and still had the same dimensions after 120 min.

If poly-asp was added, growth rates decreased to measurable levels. Also morphologies changed (see Section 3.1). Fig. 6 shows a growth sequence of a COD crystal generated in the presence of $20 \mu\text{g/ml}$ poly-asp at HIC. The crystal nucleated with one of its $\{110\}$ faces at the glass bottom of the Petri dish. The bright area in the middle of the imaged crystal is in focus, whereas the darker areas and the bright margin show crystal sections that are slightly out of the focal plane. Three minutes after starting to image the crystal, $\{100\}$ and $\{010\}$ faces are generated, which formed $\{110\}$ edges at both ends of the crystal (Figs. 6b–d). The effects of increasing poly-asp concentrations on growth of COD at HIC are shown in Fig. 7. With increasing poly-asp concentration, growth along $\langle 110 \rangle$ is inhibited and growth along $\langle 001 \rangle$ is concomitantly promoted. Because the

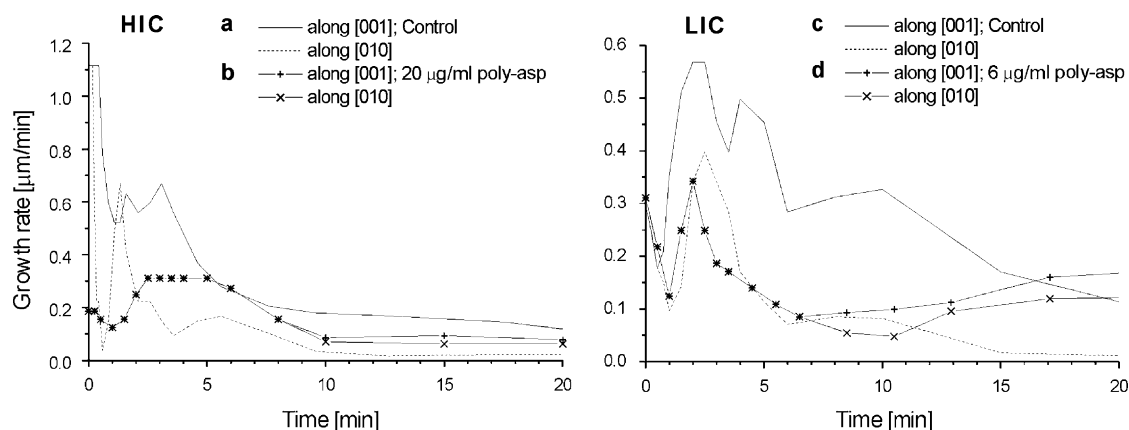


Fig. 4. Effect of supersaturation and poly-asp on growth rates of COM at HIC and LIC. The curves have been generated by derivation of crystal growth data presented in Fig. 3b, c, e, f. Error of measurement $\pm 0.05 \mu\text{m}$. (a),(c) Decreasing supersaturation results in less-frequent changes in growth rates along $[001]$ and $[010]$. (b), (d) In the presence of poly-asp these changes in growth rates were rather suppressed but, compared to COM of controls, rates increase at later stages of reactions.

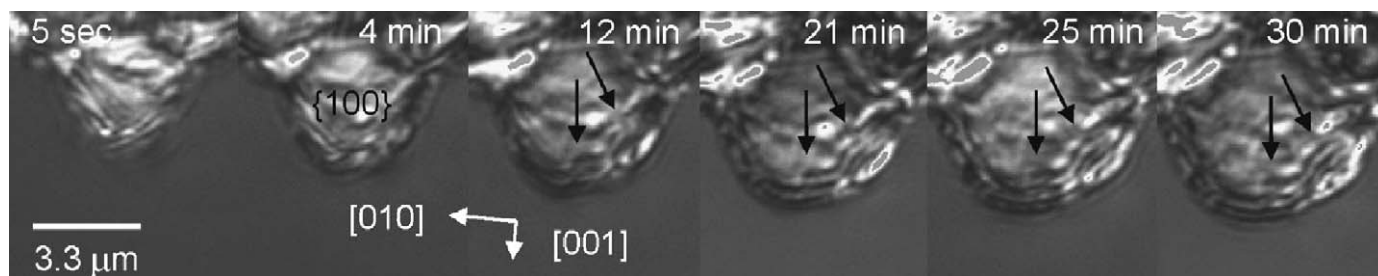


Fig. 5. SCIM image sequence of a $\{100\}$ face section of COM precipitating at LIC ($2 \mu\text{g/ml}$ poly-asp). Error of measurement $\pm 0.03 \mu\text{m}$. Start of imaging: 15 min after starting the reaction. During the initial period of growth (0–12 min), face displacement along $[001]$ and $[010]$ is associated with the generation of steps and their decay (integration of steps into the crystal matrix). At later reaction times (12–30 min), growth showed enhanced step development and increased displacement velocities along $[010]$ compared to $[001]$ directions (see area in front of the black arrows); step conversion was not observed.

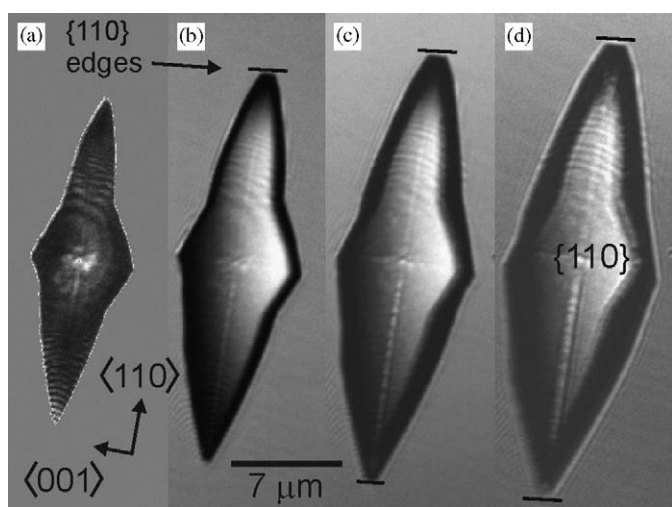


Fig. 6. SCIM image sequence of a $\{110\}$ face of COD precipitating at HIC ($20 \mu\text{g/ml}$ poly-asp). Error of measurement $\pm 0.1 \mu\text{m}$. (a) Start of imaging (5 min after starting the reaction): no indication of $\{100\}$ and $\{010\}$ faces. (b)–(d) The same crystal imaged after: (b) 3 min, (c) 10 min and (d) 30 min. Progress in overall growth, and formation of $\{110\}$ edges (black lines) caused by the generation of $\{100\}$ and $\{010\}$ faces (not visible) is apparent.

nucleation of crystals was rarely observed and because initial growth was very rapid, accurate growth rates could not be calculated. However, the growth processes and the final dimensions of the crystals were dramatically changed by poly-asp. In addition, poly-asp concentrations higher than $100 \mu\text{g/ml}$ resulted in step-like curves, a growth behavior already observed for COM (see Section 3.2.1.). A growth sequence of a COD section grown in the presence of $60 \mu\text{g/ml}$ poly-asp is shown in Fig. 8. The crystal nucleated with a face $\{0k0\}$ nearly perpendicular to $\langle 010 \rangle$ at the glass surface. The actual crystal–glass interface cannot be exactly indexed, but it is allied to $\{010\}$, because the measured angle between the planes bounding the $\{h00\}$ face is $\sim 58^\circ$, a value near to the theoretical 59.2° between $\{101\}$ faces. Because of this uncertainty, the Miller indices in Fig. 8 are put in quotation marks. The image sequence shows that growth along “ $\langle 100 \rangle$ ” is more pronounced during the first 10.5 min, whereas growth rates along “ $\langle 001 \rangle$ ” are higher between the tenth and the thirtieth minute of the elapsed time. The enhanced rates along “ $\langle 001 \rangle$ ” during the last 20 min resulted in a distinct formation of crystal edges associated with the “ $\{100\}$ ” face. The overall process of $\{100\}$ face formation is characterized by a “stop-and-go” growth at

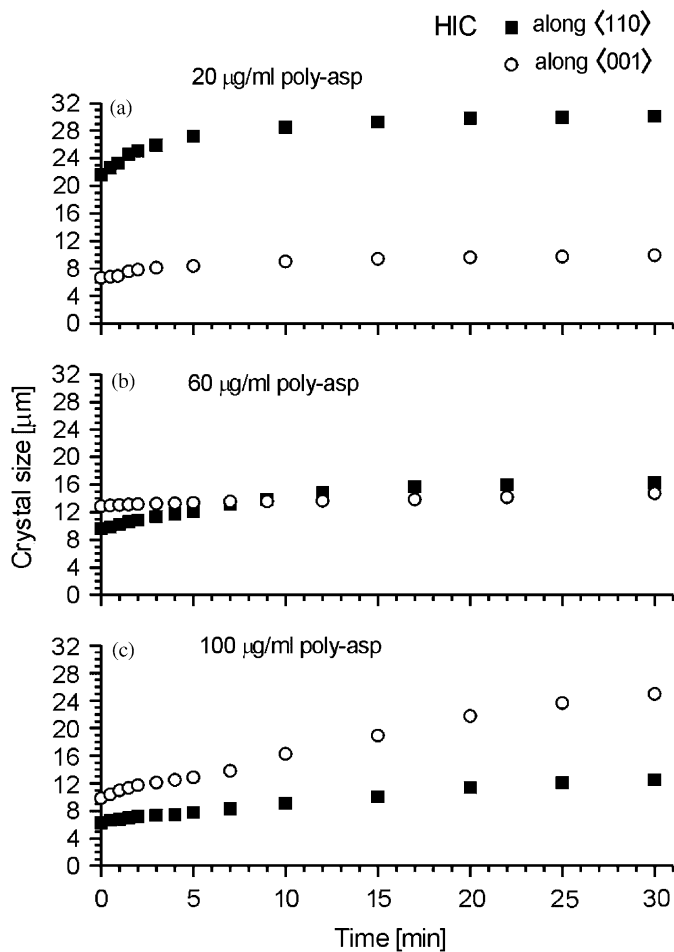


Fig. 7. Effect of poly-asp on COD growth along $\langle 110 \rangle$ and $\langle 001 \rangle$ at HIC. Error of measurement $\pm 0.06 \mu\text{m}$. (a)–(c) Increasing poly-asp concentrations inhibit growth along $\langle 110 \rangle$ and concomitantly promote growth along $\langle 001 \rangle$. (c) Poly-asp additions $\geq 100 \mu\text{g/ml}$ resulted in step-like growth curves, already observed for COM. Start of imaging: (a) 5 min, (b) 8 min, (c) 10 min after starting the reaction.

certain sites of the “ $\{100\}$ ”-crystal face. From the first 7 min of the imaged growth, it appears that gaps have to be filled first before further growth is initiated, which is one explanation for the observed step-like growth curves (Fig. 7).

At LIC, similar effects of poly-asp on COD growth were observed. However, a ~ 10 -fold lower poly-asp concentration was required to effect growth rates comparable with those of HIC-grown COD.

4. Discussion

The present study represents one of the first uses of SCIM for the investigation of fast crystallization processes and growth kinetics. The utility of this technique is demonstrated by an analysis of the effects of supersaturation and poly-asp on the precipitation of COM and COD crystals. Our findings provide proof of the concept by confirming previous studies performed using light, SCM and AFM; in addition, we present kinetic data, in

particular from individual crystals that could not be obtained by traditional methods.

4.1. Overview of crystal phases and morphologies formed

At high calcium oxalate concentrations (HIC), only COM was formed, whereas at LIC, both COM and a few COD were generated. This observation is in contrast to former studies that reported a positive correlation between COD formation and reactant concentrations [24,44]. One reason for this difference may be that the surface materials of reaction containers used in this study favor precipitation of COM.

The presence of poly-asp favored the generation of bipyramidal COD and promoted the transformation of COM morphologies using either LIC or HIC, which is in accordance with previous observations [17,24,44]. At high poly-asp additions ($\geq 60 \mu\text{g/ml}$), precipitation of tetragonal COD prisms with well-developed (100) and (010) faces was observed. Similar effects on COD growth habit have been reported using double-hydrophilic block copolymers as inhibitors [45], nonphysiological Ca/oxalate ratios and/or supersaturations [46] and in the presence of kidney epithelial cells [40,41]. With regard to COM, the precipitation of donut-like morphologies has not been described previously, although the generation of such structures is not unusual. Taubert et al. [47] and Wegner et al. [48] precipitated donut-shaped ZnO in the presence of the block copolymers poly(ethylene oxide-styrene sulfonic acid) and poly(ethylene oxide-methacrylic acid), respectively. However, the multitude of different COM morphologies shown by Millan [25] to occur in the presence of citric acid or mucin could not be detected in the present study.

The presence of poly-asp also affected the behavior of COD nucleation. COD was always generated either by forming a $\{110\}$ or a $\{100\}$ crystal–glass interface. Nucleation via other faces or noninterfacial growth, such as for COD of controls, was not observed. This behavior suggests that poly-asp adsorbed to the glass nucleates COD from $\{110\}$ or $\{100\}$ crystal planes. A similar phenomenon was previously described by Addadi and Weiner [22] for calcium carbonate crystals nucleated by aspartic acid-rich mollusk proteins. Lieske et al. [40,41] reported that the arrangement of calcium and oxalate atoms parallel to $\{100\}$ faces of COD crystals is suitable for a selective adsorption of poly-asp. Therefore, poly-asp may both nucleate and inhibit the growth of $\{110\}$ and $\{100\}$ (or $\{010\}$) planes. For COM, the dual role of polypeptides as nucleator or inhibitor has been already reported by Campbell et al. [49], who investigated the overgrowth of COM on hydroxyapatite seed crystals pre-treated with human serum albumin. The fact that higher poly-asp concentrations resulted in $\{100\}$ -interfacial growth rather than in $\{110\}$ crystal–glass interfaces in the present study suggests that the pattern of adsorbed poly-asp may depend on concentration.

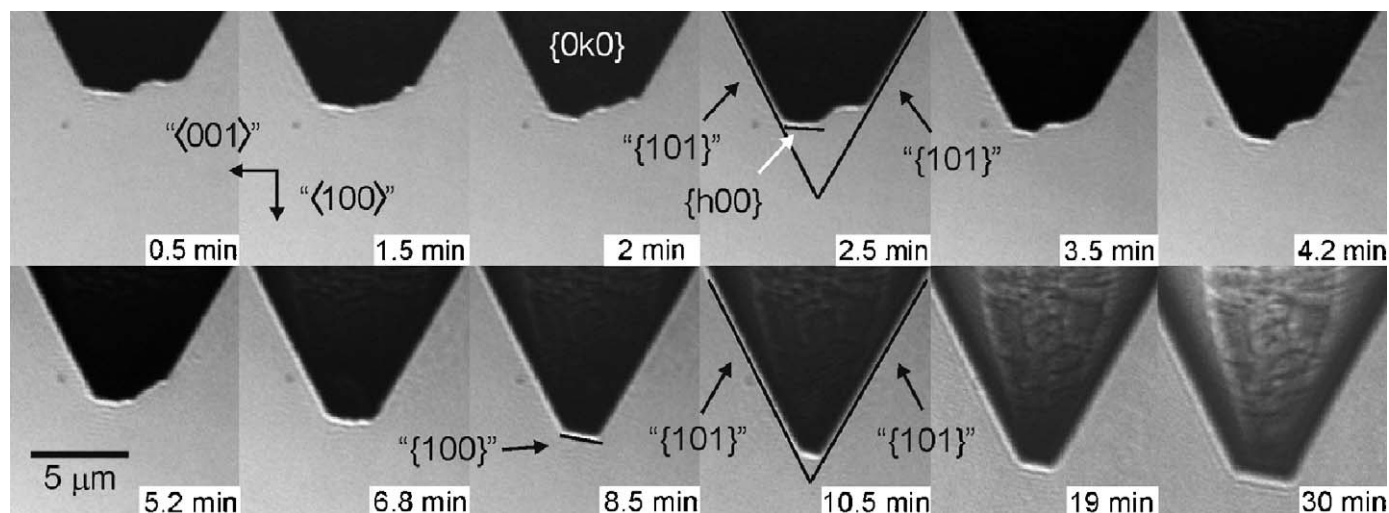


Fig. 8. SCIM image sequence of a face section of COD precipitating at HIC (60 $\mu\text{g/ml}$ poly-asp). Error of measurement $\pm 0.04 \mu\text{m}$. The dark area is in focus, whereas the bright margin is slightly out of the focal plane. Nucleation occurred with a $\{0k0\}$ face, which is allied to $\{010\}$. This is shown by the measured 58° -angle between planes (black lines) bounding the $\{h00\}$ face, a value near to the theoretical 59.2° between $\{101\}$ faces [42,43]. Because of this uncertainty, the Miller indices are set in quotation marks. Start of imaging: 16 min after starting the reaction. First 6.8 min: The imaged “ $\{100\}$ ” face formation is characterized by a growth process, where gaps have to be filled first before further growth is initiated. Last ~ 20 min: Enhanced growth along “ $\langle 001 \rangle$ ” results in a distinct and smooth crystal face.

4.2. Effect of poly-asp on the crystallization kinetics of COM

Nucleation of COM occurred throughout the entire time of the reaction (30–120 min), both in the absence and presence of poly-asp. Subsequent growth, however, was significantly affected by supersaturation and polyelectrolyte concentration.

In the absence of poly-asp, growth in the $[001]$ directions was faster than in the $[010]$ directions. Continuous slowing of growth along $[010]$ led to an aspect ratio in $[010]/[001]$ direction of ~ 0.3 , similar to that found by Guo et al. [30]. Jackson [50] and Laudise et al. [51] proposed that the relative growth rates of crystal faces depend only upon the degree of the surface roughness and the entropic state on the atomic scale; the smooth surface of a close-packed face requires defects for growth, whereas the rough surface of a less well-packed face does not, because molecules can readily be added to many sites of the surface. This may explain why the $\{010\}$ faces of COM grow more slowly than the $\{001\}$ faces.

The presence of poly-asp strongly decreased growth rates along $[001]$ at both LIC and HIC. This suggests higher adsorption rates of poly-asp at $\{001\}$ and allied faces (e.g. $\{121\}$) leading to a “poisoning” of growth sites on these faces. Growth rates parallel to $[010]$, on the other hand, increased in the presence of poly-asp, but decreased at poly-asp additions of $\geq 60 \mu\text{g/ml}$, implying a “poisoning” of growth sites on $\{010\}$ faces, too, if poly-asp concentrations are relatively high. However, the growth rates in the $[001]$ direction decreased to a greater extent than the rates along $[010]$, resulting, compared to growth in the absence of poly-asp, in increased aspect ratios along $[010]/[001]$ at the end of the elapsed time. Guo et al. [30] also found

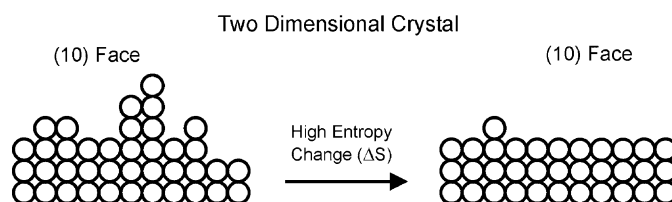


Fig. 9. Schematic drawing of a rough and a smooth crystal interface (two-dimensional crystal). The two edges are for large changes of entropy (ΔS).

increased aspect ratios for $[010]/[001]$ directions using poly-asp (12 kDa) and proposed for that effect a selective adsorption of the polypeptide to $\{001\}$ and $\{021\}$ planes, resulting in an inhibition along $[001]$. This proposal is supported by the observed characteristics of growth step and surface morphologies generated in the presence of poly-asp (Fig. 5). COM faces, which grow highly symmetrically and well faceted if unaffected, are altered by the selectivity of the polypeptide to $\{001\}$ and $\{121\}$ faces and growth steps at $\{100\}$ faces growing along $[001]$. Similarly, Jung et al. [31] reported morphological changes of growth steps and decreased growth rates parallel to $[001]$ if poly-asp was present to inhibit COM growth.

Both in the presence and absence of poly-asp, the growth curves of COM are step like. During growth, adsorbing ions will preferentially attach to the gaps in the crystal, leading to a smoothing of rough crystal faces [50–52]. This in turn leads to decreased entropic states (Fig. 9) and surface energies. A result of these processes is a decrease of face-displacement velocities and smooth curve progressions of growth rates. If, on the other hand, the ability to add ions is limited, growth can show a different behavior. It was found that discontinuous growth can be a consequence

of interface instabilities [51]. These instabilities can occur if diffusion processes are rate limiting and induce nonlinear growth [51,53]. For crystals growing in solution the entropy change is usually large, resulting in fast-growing faces which are unstable, while the more slowly growing faces are stable. A good example of this effect is found in the hydrothermal growth of quartz [21]. This limiting factor, however, becomes less important with decreasing growth rates, as indicated in Figs. 3 and 4.

The convergence of [001] and [010] growth rates observed in the presence of poly-asp suggests a “poisoning” of reaction sites at (001) and related faces by the polyelectrolyte. This growth behavior indicates a strong competition between driving forces promoting crystallization, such as supersaturation, and inhibition of crystallization by adsorbed poly-asp. The fact that higher poly-asp concentrations also inhibit the growth of {010} faces additionally argues for such a competition process. We propose that ions that diffuse at or near crystal faces will react to a high extent with adsorbed poly-asp, creating an organic/inorganic interface. Growth of such modified faces will not lead to large changes of entropy per time ($\Delta S/\Delta t$), because the liquid–solid conversion that smoothes a rough surface is strongly affected by the adsorbed poly-asp. This hypothesis is supported by the observed alternating process of the generation of growth steps and their subsequent decay (integration of steps into the crystal matrix), which only insignificantly decreased the surface roughness during growth (Fig. 5).

4.3. Effect of poly-asp on the crystallization kinetics of COD

At LIC, nucleation of COD was observed throughout the entire time of the reaction (30–120 min), independent of the absence or presence of poly-asp. At HIC, however, COD was only found if the inhibitor was present (see Sections 3.1 and 4.1).

Growth of COD in the absence of poly-asp was characterized by relatively high displacement velocities of the crystal faces. It is believed that this growth behavior results from the high symmetry of COD crystals (tetragonal), which allows the reaction system to initiate a fast assembly of the crystal structure. The mature crystal finally represents a well-faceted COD, showing very smooth surfaces.

In the presence of poly-asp, displacement velocities parallel to $\langle 110 \rangle$ or $\langle 100 \rangle$ decreased, while growth rates along $\langle 001 \rangle$ increased. This indicates a favored adsorption of poly-asp to reaction sites at {100} faces, hindering growth in $\langle 100 \rangle$ and $\langle 110 \rangle$ directions. The enhanced growth in the $\langle 001 \rangle$ direction, however, is assumed to be a result of the fact that driving forces promoting growth processes (supersaturation) compete against inhibition of growth by polyelectrolytes. On the basis of this hypothesis, it is proposed that the presence of

poly-asp leads to an environment at COD surfaces in which ions will react to a high extent with adsorbed poly-asp. Thus, the precipitation mechanism to generate COD crystals is characterized by decreased displacement velocities of crystal faces, because the liquid-to-solid conversion to smoothing a rough surface strongly depends on the adsorbed poly-asp. In addition, changes of entropy ΔS will be relatively small during growth.

Step-like growth curves observed along $\langle 110 \rangle$ and $\langle 100 \rangle$ at high poly-asp concentrations ($\geq 100 \mu\text{g/ml}$; Fig. 7c) suggest that precipitation is affected and controlled by similar processes already found for COM growth (see above). Evidence suggests that driving forces for growth, the reduction of surface roughness and supersaturation, are limited by a decreased ability of the reaction system to transport ions to growth sites of crystal faces. The transition from smooth to step-like curves requires $\sim 60 \mu\text{g/ml}$ poly-asp, which is also the concentration at which growth in the $\langle 110 \rangle$ and $\langle 001 \rangle$ directions are in balance.

It should be noted that similar inhibition processes appear to govern the formation of COM and COD. This also argues for a more general behavior of precipitation processes in solution if inhibitors are present.

5. Conclusion

Scanning confocal interference microscopy (SCIM) has been used to study the crystallization kinetics of calcium oxalate monohydrate (COM) and calcium oxalate dihydrate (COD) in the presence and absence of poly-L-aspartic acid (poly-asp). Whereas control samples generated well-faceted monoclinic COM and tetragonal COD crystals, increasing poly-asp concentrations led to a process characterized by (a) the generation of irregular growth habits such as donuts, (b) an increase in the proportion of COD crystallized, (c) an increase of particle-number density and (d) the generation of smaller particle sizes. The inhibition of COM growth by poly-asp is characterized by decreased displacement velocities in [001] directions, while rates along [010] increase. However, higher poly-asp concentrations ($> 6 \mu\text{g/ml}$ for LIC; $> 60 \mu\text{g/ml}$ for HIC) also reduced growth parallel to [010]. It is proposed that the polypeptide selectively binds to {001} and {121} faces and growth steps at {100} faces, resulting in an altered growth along [001]. In the case of COD, increasing inhibitor concentrations led to decreased rates along $\langle 110 \rangle$ and allied directions, whereas displacement velocities parallel to $\langle 001 \rangle$ increased. Step-like growth curves were demonstrated for COM, irrespective of the presence or absence of poly-asp; for COD, this occurred only at relatively high poly-asp additions ($\geq 100 \mu\text{g/ml}$). Analysis of image sequences and face-displacement rates suggest that crystal growth is strongly affected by competing and alternating effects, in which diffusion processes are rate limiting and induce nonlinear growth.

Acknowledgments

The authors thank Silvia Mittler (Department of Physics & Astronomy, University of Western Ontario, London, Ont., Canada) for the useful discussions about interference microscopy. These studies were supported by the Canadian Institutes of Health Research and the Canadian Arthritis Network.

References

- [1] D.S. Milliner, Epidemiology of calcium oxalate urolithiasis in man, in: *Calcium Oxalate In Biological Systems*, CRC Press, Boca Raton, 1995 p. 169.
- [2] W.G. Robertson, S.E. Longhorn, H.N. Whitefield, R.J. Unwin, M.A. Mansell, G.H. Neild, The changing pattern of the age of onset of urinary stone disease in the UK, in: *Kidney stones: Proceedings of the Eighth European Symposium on Urolithiasis*, Editoriale Bios, Cosenza, Italy, 1999, p. 165.
- [3] J.P. Kavanagh, L. Jones, P.N. Rao, *Clin. Sci.* 98 (2000) 151.
- [4] N.S. Mandel, G.S. Mandel, *J. Urol.* 142 (1989) 1516.
- [5] N. Mandel, R. Riese, *Am. J. Kidney Dis.* 17 (1991) 402.
- [6] A.F. Piratos, H. Khalaff, P.T. Cheng, K. Psihramis, M.A.S. Jewet, *J. Urol.* 151 (1994) 571.
- [7] K.G. Christmas, L.B. Gower, S.R. Khan, H. El-Shall, *J. Colloid Interface Sci.* 256 (2002) 168.
- [8] C.R. Scheid, L.-C. Cao, Th. Honeyman, J.A. Jonassen, *Front. Biosci.* 9 (2004) 797.
- [9] J.C. Lieske, F.G. Toback, *Curr. Opin. Nephrol. Hypertens.* 9 (2000) 349.
- [10] S.R. Khan, D.J. Kok, *Front. Biosci.* 9 (2004) 1450.
- [11] X. Martin, L.H. Smith, P.G. Werness, *Kidney Int.* 25 (1984) 948.
- [12] J.C. Lieske, F.G. Toback, *Am. J. Physiol.* 264 (1993) F800.
- [13] J.C. Lieske, M.M. Walsh-Reitz, F.G. Toback, *Am. J. Physiol.* 262 (1992) F622.
- [14] F.L. Coe, J.H. Parks, J.R. Asplin, *N. Engl. J. Med.* 327 (1992) 1141.
- [15] H. Fleisch, *Kidney Int.* 13 (1978) 361.
- [16] J.C. Lieske, R. Leonard, F.G. Toback, *Am. J. Physiol.* 268 (1995) F604.
- [17] J.A. Wesson, E.M. Worcester, J.H. Wiessner, N.S. Mandel, J.G. Kleinman, *Kidney Int.* 53 (1998) 952.
- [18] J.R. Hoyer, *Miner. Electrolyte Metab.* 20 (1994) 385.
- [19] H. Shiraga, W. Min, W.J. Van Dusen, M.D. Clayman, D. Miner, C.H. Terrell, J.R. Sherbotie, J.W. Foreman, C. Przysiecki, E.G. Nielson, J.R. Hoyer, *Proc. Nat. Acad. Sci.* 89 (1992) 426.
- [20] M. Keykhosravani, A. Doherty-Kirby, C.J. Zhang, D. Brewer, H.A. Goldberg, G.K. Hunter, G. Lajoie, *Biochemistry* 44 (2005) 6990.
- [21] E.M. Worcester, S.S. Blumenthal, A.M. Beshensky, D.L. Lewand, *J. Bone Miner. Res.* 7 (1992) 1029.
- [22] L. Addadi, S. Weiner, *Proc. Nat. Acad. Sci.* 82 (1985) 4110.
- [23] B.C. Bunker, P.C. Rieke, B.J. Tarasevich, A.A. Campbell, G.E. Fryxell, G.L. Graff, L. Song, J. Liu, J.W. Virden, G.L. Mc Vay, *Science* 264 (1994) 48.
- [24] J.A. Wesson, E. Worcester, *Scanning Microsc.* 10 (1996) 415.
- [25] A. Millan, *Crystal Growth Des.* 1 (2001) 245.
- [26] J.P. Kavanagh, *Scanning Microsc.* 6 (1992) 685.
- [27] A.L. Rogers, D. Ball, W. Harper, *Clin. Chim. Acta* 220 (1993) 125.
- [28] M. Daudon, B. Lacour, *Clin. Nephrol.* 48 (1997) 292.
- [29] S.R. Qiu, A. Wierzbicki, C.A. Orme, A.M. Cody, J.R. Hoyer, G.H. Nancollas, S. Zepeda, J.J. De Yoreo, *Proc. Nat. Acad. Sci.* 101 (2004) 1811.
- [30] S. Guo, M.D. Ward, J.A. Wesson, *Langmuir* 18 (2002) 4284.
- [31] T. Jung, X. Sheng, Ch.K. Choi, W.-S. Kim, J.A. Wesson, M.D. Ward, *Langmuir* 20 (2004) 8587.
- [32] P. Drove, private communication.
- [33] G. Sazaki, T. Matsui, K. Tsukamoto, N. Usami, T. Ujihara, K. Fujiwara, K. Nakajima, *J. Crystal Growth* 262 (2004) 536.
- [34] P. Muehlig, Th. Klupsch, U. Schell, R. Hilgenfeld, *J. Crystal Growth* 232 (2001) 93.
- [35] P. Muehlig, Th. Klupsch, U. Kaulmann, R. Hilgenfeld, *J. Struc. Biol.* 142 (2003) 47.
- [36] I. Cornelese-ten Velde, J. Bonnet, H.J. Tanke, J.S. Ploem, *Histochemie* 89 (1988) 141.
- [37] M. Born, E. Wolf, *Principles of Optics: Electromagnetic Theory of Propagation, Interference and Diffraction of Light*, seventh ed., Cambridge University Press, Cambridge, 1999.
- [38] W. Krug, J. Rienitz, G. Schulz, *Contributions to Interference Microscopy*, Hilger & Watts Ltd., London, 1964.
- [39] J.S. Ploem, F.A. Prins, I. Cornelese-ten Velde, *Reflection-contrast microscopy*, in: *Light Microscopy in Biology: A Practical Approach*, Oxford University Press, Oxford, 1999 p. 275.
- [40] J.C. Lieske, F.G. Toback, S. Deganello, *Kidney Int.* 60 (2001) 1784.
- [41] J.C. Lieske, F.G. Toback, S. Deganello, *Calcif. Tissue Int.* 58 (1996) 195.
- [42] V. Tazzoli, Ch. Domeneghetti, *Am. Mineral.* 65 (1980) 327.
- [43] Data were entered into a calculating program given in <http://www.mathe-formeln.de>.
- [44] J.A. Wesson, E.M. Worcester, J.G. Kleinman, *J. Urol.* 163 (2000) 1343.
- [45] D. Zhang, L. Qi, J. Ma, H. Cheng, *Chem. Mater.* 14 (2002) 2450.
- [46] T. Jung, W.-S. Kim, Ch.K. Choi, *Mater. Sci. Eng. C* 24 (2004) 31.
- [47] A. Taubert, D. Palms, Oe. Weiss, M.-T. Piccini, D.N. Batchelder, *Chem. Mater.* 14 (2002) 2594.
- [48] G. Wegner, P. Baum, M. Mueller, J. Norwig, K. Landfester, *Macromol. Symp.* 175 (2001) 349.
- [49] A.A. Campbell, A. Ebrahimpour, L. Perez, S.A. Smesko, G.H. Nancollas, *Calcif. Tissue Int.* 45 (1989) 122.
- [50] K.A. Jackson, *Growth and Perfection of Crystals*, Wiley, New York, 1958, p. 319.
- [51] R. A. Laudise, J.R. Carruthers, K.A. Jackson, *Annu. Rev. Mater. Sci.* 1 (1971) 253.
- [52] W. Kurz, D.J. Fisher, *Fundamentals of Solidification*, Trans Tech Publications Ltd., Uetikon-Zuerich, 1998.
- [53] J.W. Cahn, *J. Phys. Chem. Solids Suppl.* (1967) 681.